Available online at www.sciencedirect.com
ScienceDirect
Polymer 47 (2006) 7740–7746
polymer
www.elsevier.com/locate/polymer

Conductivity and mechanical properties of well-dispersed single-wall carbon nanotube/polystyrene composite

T.-E. Chang, A. Kisliuk, S.M. Rhodes, W.J. Brittain, A.P. Sokolov*

Department of Polymer Science, University of Akron, Akron, OH 44325, USA

Received 27 July 2006; received in revised form 1 September 2006; accepted 4 September 2006
Available online 25 September 2006

Abstract

The morphologies, electrical and mechanical properties and structure of polystyrene (PS) composites with varying concentrations of single-wall carbon nanotubes (SWNT) are analyzed. Using Raman spectroscopy and electron microscopy, we demonstrate that initial thermal annealing of SWNT significantly improves their dispersion in PS. In dielectric measurements, the annealed SWNT/PS composites show higher electrical conductivity and a lower percolation threshold (less than 0.3 wt%) than the raw SWNT/PS composites, which provides further evidence of good dispersion of the annealed SWNT in PS. Raman spectra of composites under tension show good transfer of an applied stress from the polymer matrix to SWNT. However, mechanical moduli of the annealed SWNT/PS composites are only increased slightly. The reason for this discrepancy remains unclear.

Keywords: Carbon nanotubes; Polystyrene; Microscopic mechanism

1. Introduction

Since the discovery of carbon nanotubes (CNT) in 1991 by Iijima [1], they have been considered as ideal reinforcing fillers in nanocomposite materials. Some key properties include high mechanical strength, high aspect ratio, small diameter, light weight, high electrical and thermal conductivities, and high thermal and air stabilities [2–13]. The mechanical properties of thermosets, such as epoxy resins [7,14–18], and thermoplastic polymers, such as poly(hydroxyaminoether) [19,20], polypropylene (PP) [21], and poly(methyl methacrylate) (PMMA) [22] have been enhanced significantly with the addition of CNT. Carbon nanotube composites also show dramatic improvements in electrical conductivity with a percolation threshold below 1% of CNT concentration [23–27]. The addition of 1 wt% multi-wall carbon nanotubes (MWNT) to polystyrene (PS) has been demonstrated to increase the elastic modulus by 42% and stress at break by 25%, in comparison to pure PS [28]. Safadi et al. also studied PS/MWNT composites, showing a 40% increase of modulus with 1 wt% concentration and a percolation threshold for conductivity at concentrations below 1 wt% [29]. These studies demonstrate the potential of CNT as a reinforcing material and indicate that the homogeneous dispersion of CNT in matrices and the mechanical load transfer from matrices to CNT are critical for their application in nanocomposite materials.

Raman spectroscopy is a powerful tool to investigate the dispersion of single-wall carbon nanotubes (SWNT) in composites, since Raman spectroscopy is a non-destructive method, it measures bulk samples and does not require special sample preparation. The two dominant features in the Raman spectra of SWNT are the radial-breathing mode (RBM) in the range of 100–300 cm^{-1} and the G-mode, so-called tangential mode (TM), at 1400–1700 cm^{-1}. The G-mode contains two main components: G^+ mode for atomic displacements along the tube axis and G^- mode for atomic displacements along the circumferential direction [30]. For metallic SWNT, the broad G^- mode is usually fitted using a Breit–Wigner–Fano (BWF) line shape that accounts for coupling of phonons

* Corresponding author. Tel.: +1 330 972 8409; fax: +1 330 972 5290.
E-mail address: alexei@uakron.edu (A.P. Sokolov).

0032-3861/$ - see front matter © 2006 Elsevier Ltd. All rights reserved.
doi:10.1016/j.polymer.2006.09.013

to the electronic continuum of the metallic tubes [31–33]. Experimental and theoretical investigations show that the BWF line strongly increases in SWNT bundles and vanishes in isolated SWNT [34,35]. Therefore, the observation of the strong BWF line in the nanotube composites indicates that SWNT remain in bundles and are not individually dispersed in the matrix.

Microscopic load transfer from the matrix to the nanotubes can be studied from the shift of the second-order Raman band (D*-band, at 2610 cm^{-1}) under applied strain or stress [7]. If the stress applied to composite material is transferred to CNT, the Raman peak shifts by a few cm^{-1} [36,37]. This shift varies linearly with applied strain in the elastic range, and the slope of the frequency–strain response depends on the orientation of the nanotubes and the properties of the polymer matrix [38,39].

The main goals of this work include (i) development of a simple sample preparation method that provides good dispersion of SWNT in a polymer matrix, and (ii) analysis of the influence of SWNT dispersion on conductivity and mechanical properties of composites. Composite microscopic structure is analyzed using Raman scattering, dielectric measurement and transmission electron microscopy (TEM). Using initial annealing of SWNT and optimum sonication time, good dispersion of SWNT in a PS matrix has been achieved. This is supported by the measurements of electrical conductivity with a low percolation threshold (less than 0.3 wt%) and the G-mode of Raman spectra. We observe a linear shift of the D* mode with stress indicating that the PS-matrix transfers stress effectively to SWNT. However, only a slight increase of mechanical modulus has been observed.

2. Experimental

2.1. Fabrication of SWNT/PS composites

Composites were made from "as provided" and annealed SWNT. The "as provided" SWNT were obtained from CarboLex Inc., which we refer to as "raw" SWNT. The annealed SWNT were thermally aged in a sand bath at 350 °C for 4 h to remove amorphous carbon. According to CarboLex Inc., the raw SWNT include approximately 35 wt% residual catalysts (Ni, Y) and 20–30 wt% amorphous carbons. Different annealing conditions, i.e., different temperatures and times, were applied. The best dispersion (according to conductivity and Raman spectroscopy analysis) was achieved by annealing at 350 °C for 4 h. This process leads to a weight loss of ~10–15%, i.e., approximately half the weight of the amorphous carbon content. Annealing at higher temperatures (up to 500 °C) did not provide any significant improvement in composite properties.

PS (M_w ~ 280,000 g/mol, Scientific Polymer Products, Inc.) and *o*-dichlorobenzene (DCB, Sigma–Aldrich) were used without purification. High molecular weight polymer was chosen for better data reproducibility of the CNT–PS composites [27]. The SWNT (annealed and/or raw) were dissolved in DCB and ultrasonicated at various times between 5 and 20 min (Ultrasonic Processor, 20 kHz) to break up the bundles. The SWNT–DCB solution was then mixed with DCB solutions of 10% PS to yield the SWNT/PS mixtures with different SWNT/PS concentrations. These solutions were homogenized by mechanical stirring and bath ultrasonication for 1 h. DCB solutions of 5% and 20% PS were also mixed with SWNT to study the effect of polymer concentration on the CNT dispersion. The conductivity and Raman data indicate that the best dispersion of SWNT was observed for the composite prepared from 10% PS solution. For comparison, the neat PS samples were made using the same procedure, but with no addition of SWNT.

The so-obtained SWNT solution was poured into a Petri dish and heated to 90–100 °C for solvent removal. These dishes were then placed into a low pressure (25 in. Hg) vacuum oven at 100 °C for ~24 h for additional solvent removal. After drying, the material was cooled to ambient temperature and then broken into smaller pieces. These pieces were then pressed into sheets with a thickness of 0.5 mm for electrical and mechanical measurements.

2.2. Measurements

Raman scattering spectra of the SWNT/PS composites were measured in backscattering geometry with a Jobin Yvon T64000 triple monochromator. A Krypton laser with a wavelength of 647 nm and power of 4 mW was used as an excitation source. Samples were placed in the mini-tensile device for measurement of Raman spectra at various levels of strain to observe the stress transfer from the polymer matrix to the CNT. Strain was varied on a time scale of seconds, however, the strain rate could not be controlled. Extension and bending strains were applied. Flexural modulus of the composite was determined by a Rheometrics Scientific Dynamic Mechanical Thermal Analyzer (DMTA) Type V instrument using a transient test and the 3-point bending geometry with a strain rate of 10^{-4}/s. The total test time was 2 min. Stress, strain, force, time and displacement data were collected. The flexural modulus was then calculated using the standard expression (ASTM D-790): $E = (l^3M)/(4Wh^3)$, here h is the thickness, W is the width of the sample, l is the span of outside supports and M is the slope of the force versus displacement (of the middle point) curve. The dielectric measurements were performed in the frequency range from 10^{-2} to 10^7 Hz using a Novocontrol Alpha broadband spectra analyzer. All measurements were performed at room temperature.

Thermogravimetric analysis (TGA) was conducted using a TA Instrument 2950. Sample weights of ~3 mg were ramped at 10 °C/min from room temperature to 900 °C under N_2 atmosphere.

The morphology of SWNT in the composite was examined by FEI Tacnai 12 transmission electron microscopy (TEM) using an accelerating voltage of 120 kV. TEM samples were prepared by depositing the SWNT/PS composite solution on a carbon-coated copper grid and evaporating the DCB solvent. For comparison, the morphology of SWNT without the PS matrix was also analyzed.

3. Results and discussion

Raman spectroscopy and TGA were used to characterize the annealed SWNT. Fig. 1 shows the Raman spectra of raw and annealed SWNT. Two Raman bands are observed in the 1250–1700 cm^{-1} range; the tangential G-band at $\nu \sim 1500$–1600 cm^{-1} and the disorder-induced D-band at $\nu \sim 1300$ cm^{-1}. It is known that the D-band is present in form of disordered sp^2 carbon containing vacancies, impurities, or other symmetry-breaking defects [29]. The large D-band peak intensity, compared with the G-band in SWNT, usually indicates the presence of amorphous carbons. After annealing the SWNT, the relative intensity of the D-band decreases slightly, indicating some removal of amorphous carbons. TGA analysis provides further evidence of the annealing effect in SWNT (Fig. 2). It is known that in annealed SWNT, oxidation begins at a higher temperature than the raw SWNT due to a smaller amount of amorphous carbons [40]. It is believed that the steeper slope for the raw SWNT indicates a larger defect density and that oxidation of the raw SWNT curve is faster. Most purification processes of SWNT [41–44] include a strong acid treatment, such as HCl or HNO_3, to remove metal catalysts. However, this strong acid treatment may damage the structure of SWNT [45], resulting in a change in intrinsic SWNT properties. Therefore, only a dry oxidation process was chosen for purification of SWNT in this study.

To maximize the modifying effects of CNT to composite properties, they should be well dispersed in the polymer matrix. Ultrasonic dispersion is one of the simplest and most convenient methods for improving the dispersion of CNT into a polymer matrix. It has been confirmed that the dispersion conditions can strongly affect the nanotube dimensions by debundling and shortening the nanotubes [46,47]. Recently, combined measurements of atomic-force microscopy (AFM) and Raman spectroscopy on individual and bundle SWNT, show that the BWF line intensity increases with bundle thickness and decreases as a result of debundling [34,35]. According to their study, the ratio of G^-(BWF) to G^+ mode intensities decreases to unity in single nanotubes.

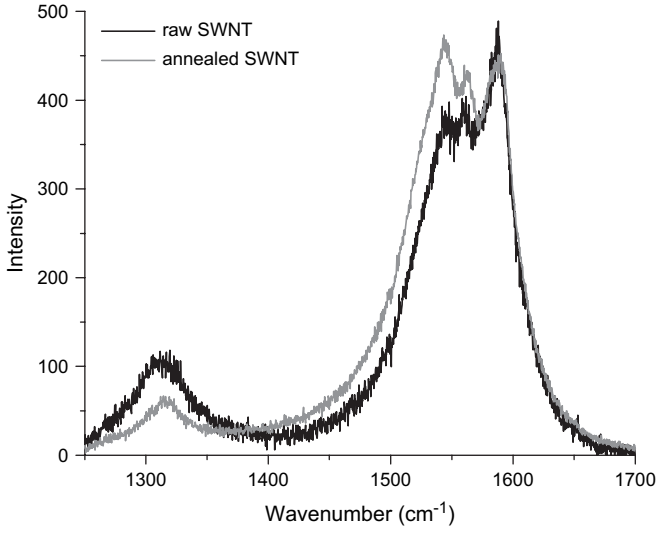

Fig. 1. Raman spectra of D-band and G-band for the raw SWNT and the annealed SWNT.

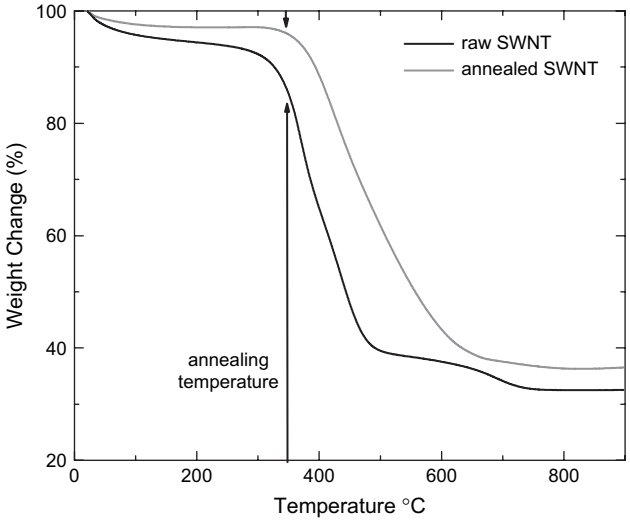

Fig. 2. TGA analysis of the raw SWNT and the annealed SWNT.

Fig. 3 compares the Raman spectra of composites made under the same conditions, except the sonication times of the annealed SWNT in DCB solvent. Fig. 3(a) shows a typical TM spectrum of SWNT bundles, indicating that the SWNT dispersed in the polymer matrix are still in bundles even after 10 min of sonication time. For the composite with 15 min sonication time, the BWF line intensity reaches the minimum (ratio of G^- to G^+ mode intensities reaches $\sim$1), suggesting that the dispersion of SWNT as single tubes is achieved most efficiently through 15 min sonication (Fig. 3(b)). The longer sonication time results in an increase in BWF mode intensity, indicating that more bundles may appear after optimum conditions are reached because of SWNT shortening (Fig. 3(c)). The degree of dispersion can be estimated from calculation of the intensity ratio of the BWF line to the G^+ line. According to the experimental results by Jiang and coworkers [34], the ratio of BWF (G^-) and G^+ line intensities

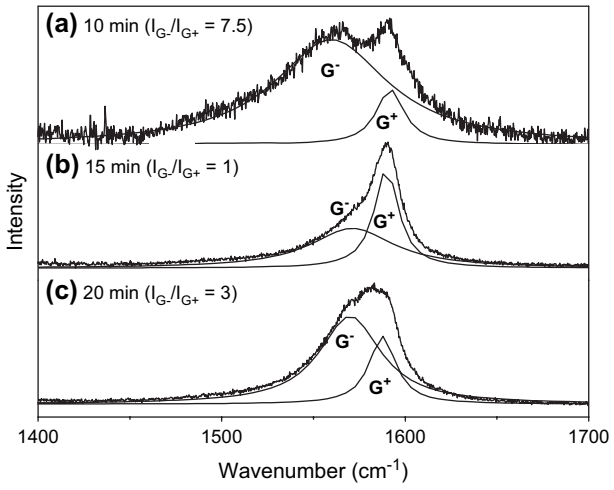

Fig. 3. TM Raman spectra of PS composites with 10 min (a), 15 min (b) and 20 min (c) sonication time for SWNT dispersion in DCB.

decreases with a decrease of the bundle size and reaches the value ~1 for the isolated metallic nanotubes. The G^-/G^+ intensities ratio for the composite of 15 min sonication time is less than 1, indicating that the majority of metallic SWNT are dispersed individually in the PS matrix under these conditions.

Both conductivity and bending modulus measurements also demonstrate their maximum values for the composite prepared with optimum sonication time, observed in Raman spectra. These results confirm the importance of good dispersion of SWNT for various properties. We noted that the optimum sonication time depends on the annealing degree of SWNT.

Upon embedding SWNT into a PS matrix, the RBM shifts slightly upward, which is generally observed in the SWNT/polymer composites due to the hydrostatic pressure on the nanotubes. Fig. 4 shows the conductivity spectra as a function of frequency for composites with different concentrations of annealed SWNT. To obtain the DC conductivity, these spectra (σ') were extrapolated to zero frequency ($\sigma_{DC} = \sigma'$ ($\omega \to 0$)), which is called the DC plateau. The DC plateau is already visible for the composite with 0.3 wt% SWNT and is clearly seen for the composites containing more than 0.5 wt% SWNT. The DC plateau values versus the SWNT concentration in the composites are plotted in Fig. 5. For comparison, the experimental results of PS composites with the raw SWNT are also shown. The conductivity of composites sharply increases at around 0.3 wt% for the annealed SWNT and at around 0.5 wt% for the raw SWNT, indicating the formation of a percolating network. To estimate the percolation threshold concentration (p_c), the experimental data were fitted using power laws for the composite conductivity near percolation threshold [48,49]:

$$\sigma_{DC} \propto (p - p_c)^t, \qquad \text{for } p > p_c \tag{1}$$

$$\sigma_{DC} \propto (p_c - p)^{-s}, \qquad \text{for } p < p_c \tag{2}$$

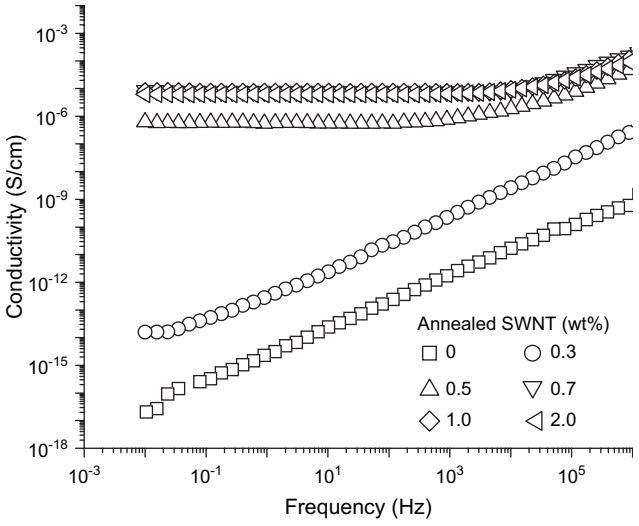

Fig. 4. Frequency dependence of σ' for PS composites with different annealed SWNT concentration.

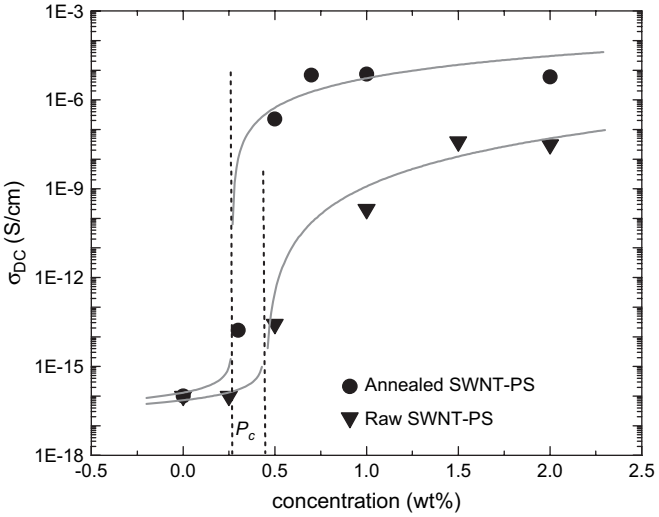

Fig. 5. DC conductivity σ_{DC} versus SWNT concentration p (wt%) for composites with the annealed SWNT and the raw SWNT. The dashed lines indicate the percolation concentration p_c, the solid lines show the fit to Eqs. (1) and (2).

where σ_{DC} is the composite conductivity, p is the SWNT weight fraction, p_c is the percolation threshold and s and t are the critical exponents. The best fits of the conductivity data (Fig. 5) give $p_c = 0.27$ and $t = 2.0$ for the annealed SWNT/PS composites and $p_c = 0.44$ and $t = 3.63$ for the raw SWNT/PS composites, indicating very low percolation thresholds. The value $t = 2.0$ for the annealed SWNT composites is in good agreement with the theoretical value of $t \sim 2.0$ for a percolation network in three dimensions [50]. The lower percolation threshold and higher conductivity for the annealed SWNT composites are the signature of better dispersion of the annealed SWNT in PS matrix, which is also confirmed by analysis of TM Raman spectra.

Fig. 6 shows the TM Raman spectra of (a) 1.0 wt% raw SWNT/PS and (b) 1.0 wt% annealed SWNT/PS composites. For the raw SWNT/PS composite, the strong BWF band

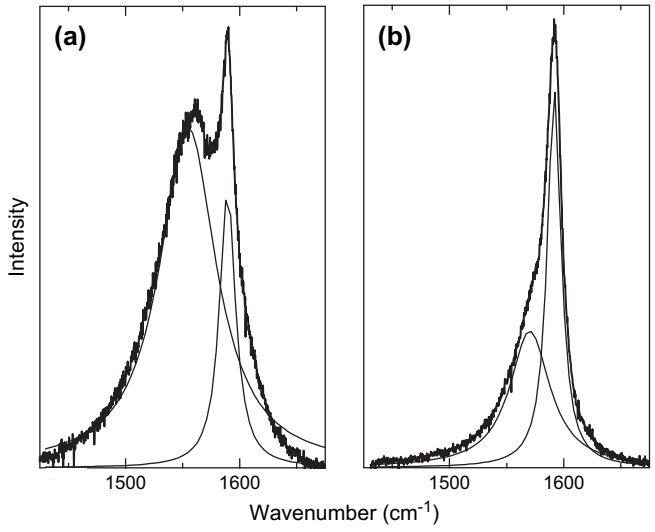

Fig. 6. TM Raman spectra of PS composites with 1.0 wt% raw SWNT (a) and 1.0 wt% annealed SWNT (b).

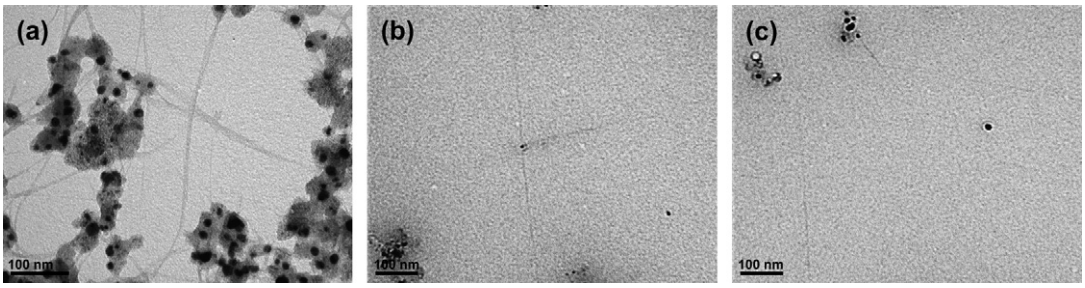

Fig. 7. TEM images of annealed SWNT (a) and PS composites with 1 wt% of annealed SWNT in different regions (b) and (c) of the same sample.

($I_{BWF}/I_G^+ \sim 4.4$) shows that SWNT in the PS matrix are dispersed in bundles. The significant decrease of relative intensity of BWF band for the annealed SWNT/PS composite ($I_{BWF}/I_G^+ \sim 1$) indicates the excellent dispersion of SWNT as single tubes after their annealing and optimum sonication time. TEM images of the annealed SWNT/PS composite support this conclusion (Fig. 7(b) and (c)).

Fig. 7(a) shows a TEM image of the annealed SWNT prepared via the deposition of the sample solution onto a carbon-coated copper grid. It appears that SWNT exist with various lengths and diameters. Moreover, significant amounts of amorphous carbons are observed even after thermal treatment of the SWNT. The morphologies of PS composites with 1 wt% annealed SWNT are shown in Fig. 7(b) and (c) for two different spots of the same sample, and confirm that SWNT are predominately dispersed as individual tubes in the composite obtained under optimum sonication conditions. Moreover, they also indicate that SWNT may connect with each other to form a conducting path in the PS matrix.

Raman spectroscopy has also been used to analyze the load transfer from the matrix to the nanotubes. The frequency of the SWNT D*-band is sensitive to stress and shifts to lower frequency under tensile stress [7]. In order to measure the stress–strain behavior and Raman spectra of D*-band at the same time, the mini-tensile testing machine was placed in the Raman spectrometer. The obtained Young's moduli of PS and SWNT/PS composites were always lower than the expected, due to the slippage of samples from the device, caused by the brittleness of PS. Therefore, the measured D*-band shift values versus strain could not present correct values due to the inaccurate values of strain. However, the D*-band shift versus applied stress presents accurate data (Fig. 8) because the value of applied stress obtained from the device is independent of sample slippage. The D*-band peak was fitted by a Lorentzian curve to estimate the position of its maximum. The Raman mode shifts linearly with stress suggesting that load is transferred to SWNT well. The initial slopes are approximately $\sim 0.43\ cm^{-1}$/MPa with no significant dependence on SWNT concentration.

The bending measurement is an appropriate method to test mechanical properties for brittle materials like PS. Fig. 9 shows the flexural moduli of neat PS and composites with different SWNT concentrations. We prepared and measured three samples for each concentration to average out a possible error from sample preparation. The moduli of composites show

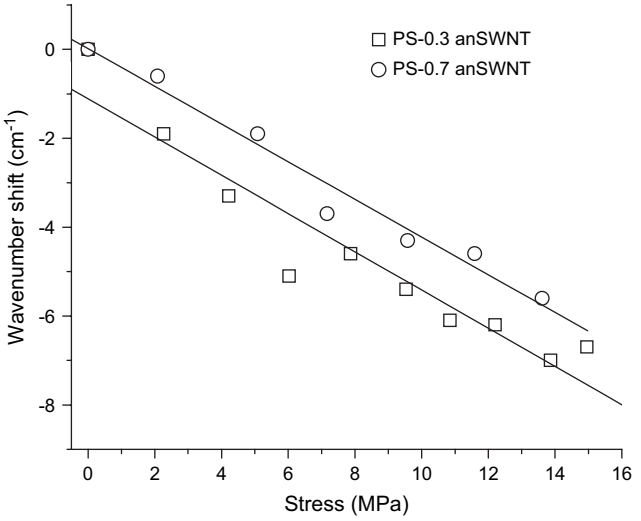

Fig. 8. Dependence of the D*-band peak position on stress in PS composites with 0.3 and 0.7 wt% annealed SWNT.

significant data scattering (Fig. 9). The overall tendency, however, demonstrates only a modest increase with SWNT concentration. Compared with the neat PS, the flexural modulus of the composite increases by about 20–30% with the addition of 2 wt% annealed SWNT.

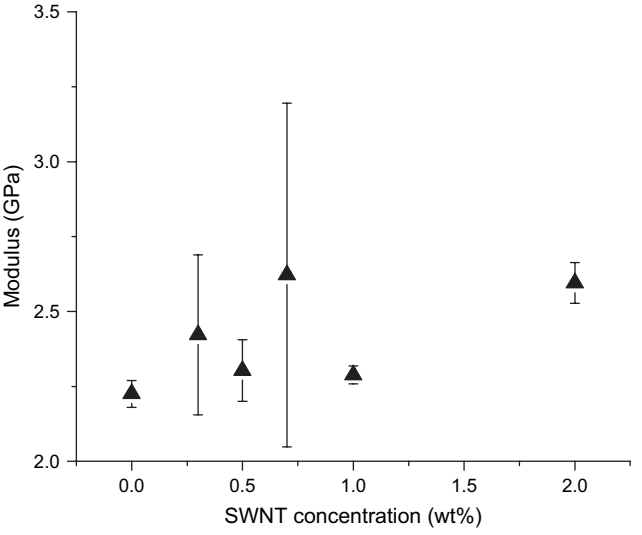

Fig. 9. Dependence of the flexural modulus on concentration of the annealed SWNT.

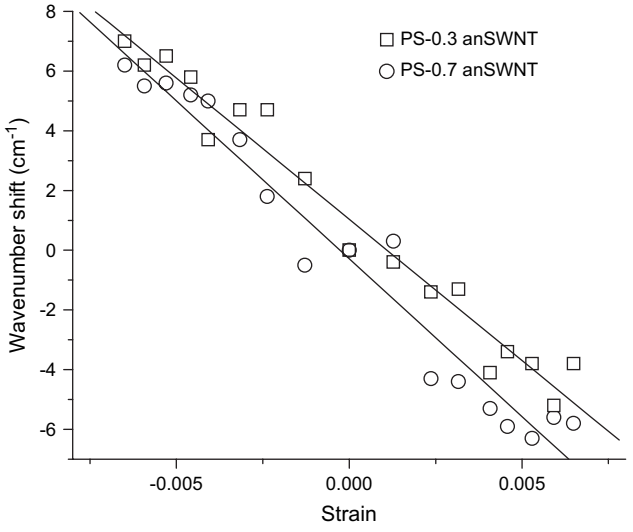

Fig. 10. Dependence of the D*-band peak position on the flexural strain for the composites with 0.3 and 0.7 wt% annealed SWNT.

We also measured the D*-band shift under applied bending strain (Fig. 10). The slopes are approximately $-950\ cm^{-1}$ per strain with no significant dependence on concentration or the sign of the strain (expansion or compression). To calculate the shift/stress values in the bending measurement we used the PS modulus (2.2 GPa). With this modulus, the slope $-950\ cm^{-1}$ per strain provides estimate of shift/stress $-0.43\ cm^{-1}$/MPa, in a very good agreement with the measured value in shift versus stress curve. Therefore, it might be concluded that there is a good stress transfer from the matrix to the nanotubes. However, it does not produce a significant enhancement of mechanical moduli.

Table 1 compares the literature data for shift/stress values of CNT composites made with various matrices with our result for SWNT/PS composites. For a urethane acrylate polymer [39], epoxy [16] and polyvinyl alcohol (PVA) [51], the shift/stress values were calculated from the measured shift/strain values using their matrix modulus. For polypropylene (PP) [21] and PS, they were obtained from shift/stress curves. It appears that the shift per strain increases mostly with an increase of the matrix modulus, suggesting that it depends on the stress transferred from the matrix to SWNT. The shift/stress values are very similar for all the presented polymer matrices, even for the functionalized SWNT composite.

One molecular dynamic simulation study analyzed the interaction of SWNT with a polymer containing aromatic rings [52]. According to this study, when the aromatic rings are positioned on the polymer backbone, the rings can align parallel to the nanotube surface and therefore provide strong interfacial adhesion. In the case of PS, the aromatic rings in the side chain rotate away from the CNT surface and the aromatic rings align parallel to each other. Therefore, PS should show weak interactions with CNT and this may be one of the reasons for the observed slight increase in mechanical strength for the PS composites. Recent analysis of mechanical properties in epoxy–SWNT composites [53] demonstrated a sharp decrease in reinforcement with increase in hardness of the epoxy matrix. The improvement of modulus dropped from ~150–200% down to below 30% when the polymer matrix modulus increased from ~0.15 GPa to ~1 GPa [53]. Using SEM images, the authors argued that interfacial interaction between the polymer and CNT is weaker in a stiff matrix. A similar mechanism might explain poor enhancement of mechanical strength in stiff PS composites compared to good improvement of mechanical properties in soft PP composites, as observed in our earlier studies [21]. Our analysis, however, shows (Table 1) that interaction of PS with SWNT is as good as for other polymers and indicates good load transfer from the stiff matrix to SWNT. Thus, the reason for the observed weak improvement in mechanical properties of well-dispersed SWNT/PS composite remains unclear.

4. Conclusions

We demonstrate that initial annealing and optimum sonication of SWNT significantly improves their dispersion in a polymer matrix. The obtained SWNT/PS composites show good improvement in electrical conductivity with a low percolation threshold, less than 0.3 wt%, indicating very good dispersion of SWNT. Raman spectra and TEM images also confirm that SWNT are individually dispersed in the PS matrix. The microscopic study of the reinforcement mechanism by

Table 1
The comparison of shift/stress values of SWNT composites for various polymer matrices

	Shift/strain (cm^{-1}/strain)	Matrix modulus (GPa)	Shift/stress (cm^{-1}/MPa)	Composite modulus (GPa)
Urethane acrylate polymer[a]	−467	1.2	−0.39	
Epoxy[b]	−700	3.1	−0.23	3.7
PVA–SWNT[c]	−261.5 (0.5 wt%)	2.4	−0.11	3.0
PVA–SOH	−369.3 (0.6 wt%)		−0.15	3.8
PP[d]	−168 (1 wt%), −228 (2 wt%)	0.34	−0.17, −0.21	0.93, 0.92
PS	−300 (0.3 wt%), −376 (0.7 wt%)	2.225	−0.43, −0.42	2.42, 2.62

[a] Composite films were mechanically tested using mini-tensile test machine.
[b] The tensile properties of composite films were measured using standard tests (ASTM D638 and D695-91 tests).
[c] Tensile testing of composite films were carried out using a Rheometric Scientific minimat tensile tester at room temperature with a 200 N load cell and a crosshead speed of 0.5 mm/min. PVA–SOH is PVA composite with OH functionalized SWNT.
[d] Composite fibers were mechanically tested using mini-tensile test machine.

SWNT using Raman spectroscopy shows linear transfer of the applied stress from the polymer matrix to SWNT. Comparison to literature data shows that stress transfer is as good as in many other polymer matrices. However, we do not find significant enhancement of mechanical strength with increasing SWNT concentration. The reason for only slight increase in mechanical modulus remains unclear.

Acknowledgments

This work has been supported in part by grants from Air Force (#F49620-02-1-0428). We thank K. U. Jeong for help with TEM measurements and R. Foster for her work during summer intern period.

References

[1] Iijima S. Nature 1991;56:354.
[2] Despres JF, Deguerre E, Lafdi K. Carbon 1995;33:87.
[3] Treacy MMJ, Ebbesen TW, Gibson JM. Nature (London) 1996;381:678.
[4] Overney G, Zhong W, Tomanek Z. Physica D 1993;27:93.
[5] Robertson DH, Brener DW, Mintmire JW. Phys Rev B 1992;45:12592.
[6] Chopra NG, Benedict LX, Crespi VH, Cohen ML, Louie SG, Zettl A. Nature (London) 1995;377:135.
[7] Wagner HD, Lourie O, Feldman Y, Tenne R. Appl Phys Lett 1998; 72:188.
[8] Iijima S, Brabec C, Maiti A, Bernholc J. J Chem Phys 1996;104:2089.
[9] Lourie O, Wagner HD. J Mater Res 1998;13:2418.
[10] Wong EW, Sheehan PE, Lieber CM. Science 1997;277:1971.
[11] Poncharal P, Wang ZL, Ugarte D, de Heer WA. Science 1999;283:1513.
[12] Meyyappan M. Carbon nanotube: science and application. Boca Raton, FL: CRC Press; 2005.
[13] Salvetat JP, Andrew G, Briggs D, Bonard JM, Basca RR, Kulik AJ. Phys Rev Lett 1999;82:944.
[14] Sandler J, Shaffer MSP, Prasse T, Bauhofer W, Schulte K, Windle AH. Polymer 1999;40:5967.
[15] Ajayan PM, Stephan O, Colliex C, Trauth D. Science 1994;265:1212.
[16] Schadler LS, Giannaris SC, Ajayan PM. Appl Phys Lett 1998;73:3842.
[17] Lourie O, Wagner HD. Appl Phys Lett 1998;73:3527.
[18] Lourie O, Cox DM, Wagner HD. Phys Rev Lett 1998;81:1638.
[19] Jin L, Bower C, Zhou O. Appl Phys Lett 1998;73:1197.
[20] Bower C, Rosen R, Jin L, Han J, Zhou O. Appl Phys Lett 1999;74:3317.
[21] Chang TE, Jensen LR, Kisliuk A, Pipes RB, Pyrz R, Sokolov AP. Polymer 2005;46:439.
[22] Haggenmueller R, Gommans HH, Rinzler AG, Fischer JE, Winey KI. Chem Phys Lett 2000;330:219.
[23] Bai JB, Allaoui A. Composites Part A 2003;34:689.
[24] Nogalaes A, Broza G, Roslaniec Z, Schutle K, Sics I, Hsiao BS, et al. Macromolecules 2004;37:7669.
[25] Potschke P, Abdel-Goad M, Alig I, Dudkin S, Lellinger D. Polymer 2004;45:8863.
[26] Benoit JM, Corraze B, Lefrant S, Blau W, Bernier P, Chauvet O. Synth Met 2001;121:215.
[27] Ramasubramaniam R, Chen J, Liu H. Appl Phys Lett 2003;83:928.
[28] Quin D, Dickey EC, Andrews R, Rantell T. Appl Phys Lett 2000;76: 2868.
[29] Safadi B, Andrews R, Grulke EA. J Appl Polym Sci 2002;84:2660.
[30] Jorio A, Pimenta MA, Souza Filho AG, Saito R, Dresselhaus G, Dresselhaus MS. New J Phys 2003;5:139.1.
[31] Kataura H, Kumazawa Y, Maniwa Y, Umezu I, Suzuki S, Ohtsuka Y, et al. Synth Met 1999;103:2555.
[32] Pimenta MA, Marucci A, Empedocles S, Bawendi M, Hanlon EB, Rao AM, et al. Phys Rev B 1998;58:R16016.
[33] Brown SDM, Jorio A, Corio PR, Dresselhaus MS, Dresselhaus G, Saito R, et al. Phys Rev B 2001;63:155414.
[34] Jiang C, Kempa K, Zhao J, Schlecht U, Kolb U, Basche T, et al. Phys Rev B 2002;66:161404.
[35] Paillet M, Poncharal Ph, Zahab A, Sauvajol J-L. Phys Rev Lett 2005;94: 237401.
[36] Wood JR, Zao Q, Frogley MD, Meurs ER, Prins AD, Peijs T, et al. Phys Rev B 2000;62:7571.
[37] Wood JR, Wagner HD. Appl Phys Lett 2000;76:2823.
[38] Wood JR, Frogley MD, Meurs ER, Prins AD, Peijs T, Dunstan DJ, et al. J Phys Chem B 1999;10:10388.
[39] Wood JR, Zao Q, Wagner HD. Composites Part A 2001;32:391.
[40] Watts PCP, Hsu W-K, Kroto HW, Walton DRM. Nano Lett 2003;3:549.
[41] Rinzler AG, Liu J, Nikolaev P, Huffman CC, Rodriguez-Macias FJ, Boul PJ, et al. Appl Phys A 1998;67:29.
[42] Hu H, Zhao B, Itkis ME, Haddon RC. J Phys Chem B 2003;107:13838.
[43] Harutyunyan AR, Pradhan BK, Chang JP, Chen G, Eklund PC. J Phys Chem B 2002;106:8671.
[44] Chiang IW, Brinson BE, Smalley RE, Margrave JL, Haune RH. J Phys Chem B 2001;105:1157.
[45] Monthioux M, Smith BW, Burteaux B, Claye A, Fisher JE, Luzzi DE. Carbon 2001;39:1251.
[46] Islam MF, Rojas E, Bergey DM, Johanson AT, Yodh AG. Nano Lett 2003;3:269.
[47] O'Connell MJ, Bachilo SM, Huffman C, Moore VC, Strano MS, Haroz E, et al. Science 2002;297:593.
[48] Kirkpatrick S. Rev Mod Phys 1973;45:574.
[49] Stauffer D, Aharony A. Introduction to percolation theory. London: Taylor and Francis; 1992.
[50] Sahimi M. Applications of percolation theory. London: Taylor and Francis; 1994.
[51] Liu L, Barber AH, Nuriel S, Wagner HD. Adv Funct Mater 2005;15:975.
[52] Yang M, Koutos V, Zaiser M. J Phys Chem B 2005;109:10009.
[53] Ci L, Bai J. Compos Sci Technol 2006;66:599.